Reluctance of a neutral nanoparticle to enter a charged pore

Sebastian Getfert, Thomas Töws, and Peter Reimann
Fakultät für Physik, Universität Bielefeld, 33615 Bielefeld, Germany
(Received 3 July 2013; revised manuscript received 6 September 2013; published 15 November 2013)

We consider the translocation of a neutral (uncharged) nanoparticle through a pore in a thin membrane with constant surface charge density. If the concomitant Debye screening layer is sufficiently thin, the resulting forces experienced by the particle on its way through the pore are negligible. But when the Debye length becomes comparable to the pore diameter, the particle encounters a quite significant potential barrier while approaching and entering the pore, and symmetrically upon exiting the pore. The main reason is an increasing pressure, which acts on the particle when it intrudes into the counter ion cloud of the Debye screening layer. In case the polarizability of the particle is different (usually smaller) than that of the ambient fluid, a second, much smaller contribution to the potential barrier is due to self-energy effects. Our numerical treatment of the problem is complemented by analytical approximations for sufficiently long cylindrical particles and pores, which agree very well with the numerics.

DOI: 10.1103/PhysRevE.88.052710 PACS number(s): 87.16.dp, 87.15.A−, 87.50.ch

I. INTRODUCTION

How can a charged object exert electric forces on an uncharged object? Generally speaking, this may be the case whenever the nominally neutral object and/or its overall neutral environment is actually composed of positive and negative constituents, which may freely move (e.g., ions in a liquid) or lead to dielectric polarization effects (e.g., electrons and protons in a solid) in the presence of an electric field, see Fig. 1.

According to textbook electrostatics [1], any given charge in a polarizable environment gives rise to a so-called self-energy or energy of charge, which is negative and proportional to the polarizability of the environment. As a consequence, a repulsive force between the given charge and any other extended object arises in the most common case that they are both surrounded by a fluid and the polarizability of the object is lower than that of the fluid, see Fig. 1(a).

One of the best known examples is an ion (charged object) in an aqueous solution (dielectric constant of water $\epsilon_w \approx 80$) being repelled by a biological or artificial membrane (neutral object) with a typical dielectric constant ϵ_m of $2-5$ [2–6]. Here, we address the conceptually analogous case of the potential barrier, which an uncharged particle encounters upon entering a charged membrane pore. The corresponding forces on the particle are closely related to the well-known phenomenon of dielectrophoresis and will henceforth be denoted as dielectric forces.

Additional important effects arise in the usual case that the ambient fluid contains positively and negatively charged ions [3–6]. As a consequence, any charged object now attracts counterions (and repels coions) from the ambient fluid (electric double layer). The characteristic extension of such a counterion layer or cloud is quantified by the so-called Debye length, typically of the order of 1 nm. At distances beyond a few Debye lengths, the charged object is thus essentially screened, i.e., it looks as if it were uncharged.

On the one hand, the above mentioned dielectric forces are therefore expected to be notably reduced already within the counterion layer and become negligible outside it. On the other hand, additional repulsive forces are expected when an uncharged object enters the electric double layer, see Fig. 1(b). The reason is that the prevailing like-charged ions repel each other, resulting in an excess pressure within the counterion cloud, which also acts against any intruding object. While this effect bears some resemblance to osmotic pressure [7], the term counterion pressure seems more appropriate to us and will be adopted from now on.

A detailed exploration of those effects is the main subject of our present work. In particular, we will demonstrate that, under typical experimental conditions, the counterion pressure gives rise to considerably larger energy barriers against the entrance of uncharged nanoparticles into charged nanopores than the dielectric forces.

II. MODEL

A fluid chamber is divided into two compartments by a thin biological or solid-state membrane (typical thickness $H \approx 20$ nm) with a cylindrical pore (typical radius $Q \approx 5$ nm),[1] see Fig. 1 and Refs. [8–15]. The fluid chamber contains an electrolyte solution with N_ν different ionic species and preset bulk concentrations $c_{\nu,0}$ (far away from the membrane). Typical experimental concentrations $c_{\nu,0}$ range from about 10 mM to about 1000 mM [8–16]. The membrane is modeled as an insulator with constant surface charge density σ, whose quantitative value depends on the membrane material, pH value, salt concentrations, and other factors, and which is screened by counterions in the electrolyte solution. Under typical experimental conditions the surface charge density σ is of the order of $\sigma = -50\ \mathrm{mC/m^2}$ [17–22].

An uncharged, prolate particle of radius $R < Q$ and length $L \geqslant 2R$ is contained in the electrolyte solution. In our model, the particle is a cylinder with half spheres merged to the ends, and hence the particle becomes a sphere if $L = 2R$. Typical values in our examples below will be $R = 3$ nm and $L =$ 6–60 nm. The quantity of foremost interest is the net force acting on the particle due to the counterion pressure and the dielectric forces mentioned in Sec. I.

[1]For the sake of both numerical convenience and a more realistic modeling, the corners of the pore in Fig. 2 are in fact slightly rounded (1 nm curvature radius).

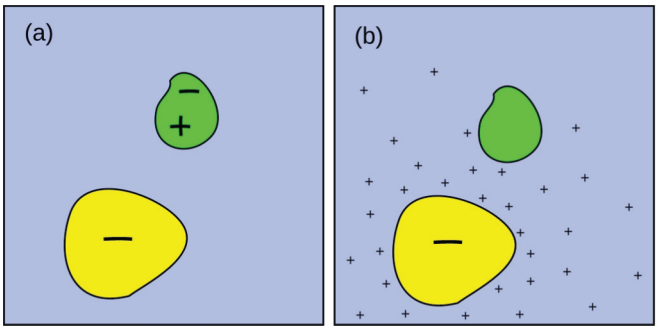

FIG. 1. (Color online) Interaction forces between a negatively charged and an electrically neutral object. (a) Dielectric forces: The charged object induces a polarization (electric dipole) in the nominally neutral object, resulting in an attraction between the two objects in vacuum. In the presence of an ambient aqueous solution, whose polarizability (permittivity) is higher than that of the neutral object, the net result is a repulsion between the two objects. (b) Counterion pressure: The negatively charged object attracts positive counterions from the ambient electrolyte solution. The neutral object is repelled by the increased pressure within the counterion cloud (caused by the mutual repulsion of the counterions). Analogous considerations apply for a positively instead of a negatively charged object.

From the viewpoint of the numerical (and analytical) tractability of the problem, two further assumptions are practically unavoidable [6,23–25], see also Sec. III E. First, we restrict our discussion to the axisymmetric case where a particle translocates through the pore along the z axis (see Fig. 2). This will also be justified by our later finding that the neutral particle is repelled by the uniformly charged membrane and pore surfaces and hence the energetically most favorable translocation path (e.g., driven by thermal noise) will be along the pore axis [19,25–28]. Second, we restrict ourselves to steady-state (time-independent) situations, and we assume, similarly as in Refs. [6,25,27,28], that the particle itself does not to exhibit any notable proper motion within the relaxation time of its environment. In other words, the particle position is a model parameter rather than a dynamical variable. The justification is, as usual, the clear-cut time- and length-scale separation between the nanoparticle and the molecular degrees of freedom of the ambient fluid [5,6,29].

III. GENERAL FRAMEWORK

A. Basic equations

In this section we summarize the Poisson, Nernst-Planck, and Stokes equations. A more detailed discussion is provided, e.g., in Refs. [16,30–32].

The electric potential ψ obeys the Poisson equation

$$-\epsilon_0 \nabla \cdot [\epsilon(\mathbf{x}) \nabla \psi(\mathbf{x})] = \rho(\mathbf{x}) + \rho_m(\mathbf{x}), \tag{1}$$

where ϵ_0 is the vacuum permittivity and ϵ the dielectric constant (relative permittivity). While the static charge density ρ_m is associated with the fixed membrane surface charges, ρ denotes the local charge density due to the mobile ions,

$$\rho(\mathbf{x}) := \begin{cases} e_0 N_A \sum_{\nu=1}^{N_\nu} Z_\nu c_\nu(\mathbf{x}) & \text{in the electrolyte solution} \\ 0 & \text{else} \end{cases} \tag{2}$$

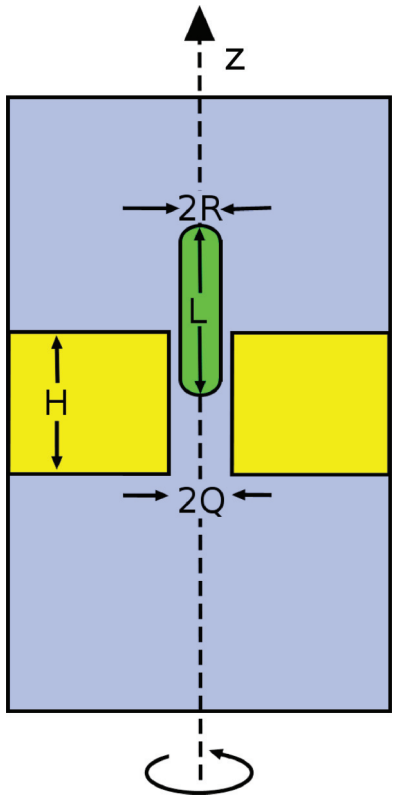

FIG. 2. (Color online) Schematic illustration of the model. A membrane of thickness H separates two reservoirs which are filled with electrolyte solution and connected by a cylindrical nanopore of radius Q. A prolate particle with radius R and length L translocates through the pore along the z axis (dashed line). The complete setup is rotationally symmetric about the z axis, whose origin ($z = 0$) is at the pore center.

Here, $e_0 = 1.602\ldots \times 10^{-19}$ C is the elementary charge and $N_A = 6.022\ldots \times 10^{23}$/mol is Avogadro's constant. Furthermore, Z_ν and c_ν denote the valence and the molar concentration of the ν^{th} ionic species.

The particle flux density $\mathbf{J}_\nu$ of the νth ionic species consists of three different contributions, arising from (i) convection due to the velocity field of the fluid $\mathbf{u}$, (ii) concentration gradients, and (iii) the electric field $\mathbf{E} = -\nabla\psi$, and is given by the Nernst-Planck equation

$$\mathbf{J}_\nu(\mathbf{x}) = c_\nu(\mathbf{x})\mathbf{u}(\mathbf{x}) - D_\nu \nabla c_\nu(\mathbf{x}) - \mu_\nu c_\nu(\mathbf{x})\, \nabla\psi(\mathbf{x}). \tag{3}$$

The diffusion coefficient D_ν is related to the mobility μ_ν via $\mu_\nu = Z_\nu e_0 D_\nu / k_B T$, where k_B denotes Boltzmann's constant and T the temperature. Assuming a steady state, particle number conservation implies

$$\nabla \cdot \mathbf{J}_\nu(\mathbf{x}) = 0. \tag{4}$$

The velocity field $\mathbf{u}$ and the pressure p of the electrolyte solution are governed by the Navier-Stokes equation. Since in our present case the Reynolds number is very low, the nonlinear terms in this equation can be safely neglected. Focusing on steady states and neglecting the very small effect of gravity, it is thus sufficient to solve the simpler Stokes equation

$$\eta\, \Delta\mathbf{u}(\mathbf{x}) - \nabla p(\mathbf{x}) - \rho(\mathbf{x})\nabla\psi(\mathbf{x}) = \mathbf{0}, \tag{5}$$

with η the viscosity of the fluid. Analogously to Eq. (4), assuming an incompressible fluid and focusing on steady-state solutions, mass conservation implies

$$\nabla \cdot \mathbf{u}(\mathbf{x}) = 0. \tag{6}$$

B. Parameters and boundary conditions

The relative permittivity is assumed to be of the form

$$\epsilon(\mathbf{x}) = \begin{cases} \epsilon_w & \text{in the electrolyte solution} \\ \epsilon_m & \text{in the membrane} \\ \epsilon_p & \text{in the particle} \end{cases}. \tag{7}$$

While ϵ_w is usually close to the value $\approx$80 for water at room temperature, ϵ_m and ϵ_p are material dependent. A typical value for biological matter is $\epsilon = 2$ and for solid-state membranes (e.g., SiO_2, SiN, Si_3N_4) $\epsilon = 5$ [2–7,33–36]. Typical particle permittivities ϵ_p are in the same range and actually turn out to play a very minor role. Thus, we will usually adopt the following choices: $\epsilon_w = 80$ and $\epsilon_m = \epsilon_p = 5$.

With respect to the static (fixed) surface charges we can, as detailed in Refs. [1,6], formally set $\rho_m = 0$ in Eq. (1) and instead work with the boundary conditions

$$\psi(\mathbf{x}) \text{ continuous}, \tag{8}$$

$$[\epsilon_w \nabla\psi_w(\mathbf{x}) - \epsilon_m \nabla\psi_m(\mathbf{x})] \cdot \mathbf{n}(\mathbf{x}) = -\sigma/\epsilon_0, \tag{9}$$

$$[\epsilon_w \nabla\psi_w(\mathbf{x}) - \epsilon_p \nabla\psi_p(\mathbf{x})] \cdot \mathbf{n}(\mathbf{x}) = 0, \tag{10}$$

where ψ_w, ψ_m, and ψ_p denote the electric potential at the respective side of the interface [see also Eq. (7)] and where $\mathbf{n}$ is the normal vector pointing from the membrane and the particle, respectively, into the electrolyte solution. The remaining boundary conditions for the Poisson equation (1) are chosen as $\psi(\mathbf{x}) = 0$ at the top and bottom walls of the cylindrical fluid chamber in Fig. 2 and $\nabla\psi(\mathbf{x}) \cdot \mathbf{n}(\mathbf{x}) = 0$ at the cylindrical side wall.

Turning to the Nernst-Planck equation (3), the concentrations c_ν of the different ionic species are required to assume their bulk values $c_{\nu,0}$ at the top and bottom walls of the fluid chamber. On the membrane and particle walls as well as on the cylindrical side wall of the fluid chamber, we impose insulation (or reflecting) boundary conditions $\mathbf{J}_\nu(\mathbf{x}) \cdot \mathbf{n}(\mathbf{x}) = 0$. In the following, we restrict our discussion to so-called symmetric $Z:Z$ electrolytes, i.e., $N_\nu = 2$, $Z_1 = -Z_2 =: Z$, and $c_{1,0} = c_{2,0} =: c_0$. Moreover, in our numerical examples below we will focus on the simplest case $Z = 1$. We further adopt a typical temperature $T = 300$ K and typical diffusion coefficients $D_1 = D_2 =: D = 2 \times 10^{-9}\text{m}^2/\text{s}$ [16]. Accordingly, the Debye length, quantifying the extension of the electric double layer (see also Secs. I and IV A) takes the form [16]

$$\lambda_D = \sqrt{\frac{\epsilon_0 \epsilon_w k_B T}{2 e_0^2 N_A c_0}} \simeq \sqrt{1000\,\text{mM}/c_0}\; 0.305\,\text{nm}. \tag{11}$$

With respect to the Stokes equation (5), our first assumption is that the usual no-slip boundary conditions $\mathbf{u} = \mathbf{0}$ are satisfied on the membrane and particle walls as well as on the cylindrical side wall of the fluid chamber (see Fig. 2). Concerning the top and bottom walls of the fluid chamber, we require that the pressure p approaches some preset bulk value p_0,

$$p(\mathbf{x}) = p_0. \tag{12}$$

Since only the gradient of p matters [see Eq. (5)], we can and will set

$$p_0 = 0 \tag{13}$$

without loss of generality. Moreover, we require that the normal component of the hydrodynamic stress (see, e.g., [32] for a more detailed discussion) vanishes at the top and bottom walls of the fluid chamber,

$$[-p(\mathbf{x}) + \eta(\nabla\mathbf{u}(\mathbf{x}) + [\nabla\mathbf{u}(\mathbf{x})]^T)]\mathbf{n}(\mathbf{x}) = \mathbf{0}, \tag{14}$$

where $\nabla\mathbf{u}$ denotes the matrix with elements $\partial u_i/\partial x_j$ and $[\nabla\mathbf{u}]^T$ the transposed matrix. The boundary conditions (12)–(14) are well known to be numerically stable provided the boundaries are sufficiently far away from the nanopore [37,38]. Quantitatively, we found that for not too large particle lengths ($L \lesssim H$), and not too low concentrations ($c_0 \gtrsim 1$ mM), finite-size effects become negligible for fluid chambers (see Fig. 2) beyond a radius of about 40 nm and a height of about 100 nm. For larger particle lengths or lower concentrations, the size of the fluid chamber was increased, so that finite-size effects were again negligible.

For all examples, the viscosity of water at room temperature takes its standard value $\eta = 10^{-3}$ Pa s and the values of the remaining parameters will be specified later.

C. Forces on the particle

The force $\mathbf{F}$ acting on the particle in Fig. 2 can be decomposed into two contributions [32], one arising from the interaction with the electric field $\mathbf{E} = -\nabla\psi$, and the other from the hydrodynamic interaction with the surrounding electrolyte solution,

$$\mathbf{F} = \mathbf{F}_e + \mathbf{F}_h. \tag{15}$$

The electrostatic force $\mathbf{F}_e$ can be calculated quite generally [1,7] by integrating the Maxwell stress tensor over the particle surface $\mathcal{O}(P)$,

$$\mathbf{F}_e = \epsilon_w \epsilon_0 \oint_{\mathcal{O}(P)} \left(\mathbf{E}(\mathbf{x})\,[\mathbf{E}(\mathbf{x})]^T - \frac{1}{2}|\mathbf{E}(\mathbf{x})|^2 \right) \mathbf{n}(\mathbf{x}) dS. \tag{16}$$

Similarly, the hydrodynamic force $\mathbf{F}_h$ follows by integrating the hydrodynamic stress tensor (also called pressure tensor) over the particle surface,

$$\mathbf{F}_h = \oint_{\mathcal{O}(P)} (-p(\mathbf{x}) + \eta\{\nabla\mathbf{u}(\mathbf{x}) + [\nabla\mathbf{u}(\mathbf{x})]^T\})\mathbf{n}(\mathbf{x}) dS. \tag{17}$$

If $\epsilon_p = \epsilon_w$, the net electric force $\mathbf{F}_e$ on the particle must vanish. Physically, this follows by observing that for an overall constant ϵ, the electric field is proportional to the field for $\epsilon = 1$, i.e., for a nonpolarizable particle in vacuum. Since there are no dielectric forces in the latter case, the same applies to the former case. [$\mathbf{F}_e$ in Eq. (16) must be zero in both cases.] Formally, the same follows from Poisson's equation (1), whose right-hand side vanishes within the particle region, the boundary conditions (8), (10), which imply a smooth behavior of $\mathbf{E}$ across the particle boundary for $\epsilon_p = \epsilon_w$, and by employing the Gauss theorem in Eq. (16). For a neutral

particle with arbitrary ϵ_p it thus seems justified to henceforth identify $\mathbf{F}_e$ with the dielectric forces due to polarization or self-energy effects from Fig. 1(a) and Sec. I.

D. Simplifications at thermal equilibrium

Since we are considering an isolated system (no external forces are acting) and we focus on steady-state solutions, this steady state must be tantamount to thermal equilibrium. Hence all macroscopic fluxes in the system must vanish, i.e.,

$$\mathbf{u}(\mathbf{x}) = \mathbf{0} \quad \text{and} \quad \mathbf{J}_\nu(\mathbf{x}) = \mathbf{0}. \tag{18}$$

As a consequence, all boundary conditions involving $\mathbf{J}_\nu$ and $\mathbf{u}$ are automatically fulfilled. Furthermore, the Nernst-Planck equation (3) is formally solved by the Boltzmann distribution

$$c_\nu(\mathbf{x}) = c_{\nu,0} \exp\left(- \frac{Z_\nu e_0 \psi(\mathbf{x})}{k_\mathrm{B} T} \right), \tag{19}$$

while Eq. (4) is trivially satisfied. Likewise, the Stokes equation (5) with boundary conditions (12) and (13) can be formally integrated, yielding for the pressure the result

$$p(\mathbf{x}) = 2 k_\mathrm{B} T N_\mathrm{A} c_0 \left[\cosh\left(\frac{Z e_0 \psi(\mathbf{x})}{k_\mathrm{B} T} \right) - 1 \right]. \tag{20}$$

The only remaining equation is thus Poisson's equation (1). Concerning the two charge density terms which appear on the right hand side of this equation (1) we observe that: (i) Exploiting (19), the ion charge density (2) in a $Z:Z$ electrolyte solution [see above Eq. (11)] can be rewritten as

$$\rho(\mathbf{x}) = -2 Z e_0 N_\mathrm{A} c_0 \sinh\left(\frac{Z e_0 \psi(\mathbf{x})}{k_\mathrm{B} T} \right). \tag{21}$$

(ii) The fixed membrane surface charges ρ_m are effectively accounted for by the boundary conditions (8)–(10). By combining (1) and (21), we are thus left with the so-called Possion-Boltzmann equation for the electric potential ψ

$$\epsilon_0 \nabla \cdot \left[\epsilon(\mathbf{x}) \nabla \psi(\mathbf{x}) \right] = 2 Z e_0 N_\mathrm{A} c_0 \sinh\left(\frac{Z e_0 \psi(\mathbf{x})}{k_\mathrm{B} T} \right). \tag{22}$$

Once this equation with (7)–(10) is solved, the concentration, pressure, and charge density fields immediately follow from (19)–(21).

Turning to the forces, we first remark that $\mathbf{F}_h$ from (17) simplifies to the familiar pressure integral

$$\mathbf{F}_h = - \oint_{\mathcal{O}(P)} p(\mathbf{x})\, \mathbf{n}(\mathbf{x}) dS. \tag{23}$$

In other words, $\mathbf{F}_h$ quantifies the counterion pressure effects from Fig. 1(b) and Sec. I.

Furthermore, for symmetry reasons the force $\mathbf{F}$ resulting from (15), (16), (23) will be parallel to the pore axis. Henceforth, this force component is denoted by $F(z)$ for any given position z of the particle center in Fig. 2. Finally, the corresponding potential energy $U(z)$, from which $F(z)$ derives, follows as

$$U(z) = - \int_{z_0}^{z} dz'\, F(z'), \tag{24}$$

where z_0 denotes the particle position when it touches the bottom wall in Fig. 2. Symmetry reasons further imply that

$$F(-z) = -F(z). \tag{25}$$

With (24) we thus can conclude that

$$U(-z) = U(z). \tag{26}$$

E. Numerical method

In spite of the above mentioned simplifications at thermal equilibrium, the remaining Poisson-Boltzmann equation (22), complemented by (7)–(10), and the final surface integrations in Eqs. (16) and (23) can only be tackled analytically in a few special cases and within certain approximations, see, e.g., Sec. IV. In all other cases, only numerical solutions are possible. It, however, turns out that the numerical treatment of the fully three-dimensional problem is still very demanding, even on modern computers, if a satisfactory numerical accuracy is required. Consequently, similar previous studies are restricted to one-dimensional [35], two-dimensional [25], or axisymmetric problems [24,39–42] problems. In the latter case, which is also at the focus of our present work, an effectively two-dimensional problem is readily recovered when going over to cylindrical coordinates (see, e.g., Ref. [32] for the explicit expressions). Our numerical results presented below were obtained using the commercial COMSOL 4.3A MULTIPHYSICS package of coupled partial differential equation solvers, exploiting finite element methods [38].

IV. ANALYTICAL APPROXIMATIONS

For a very long particle ($L \gg H$ in Fig. 2), which is fully threaded through the pore so that both ends stick far out at either side of the pore, we are dealing with an almost translation invariant situation and the net force on the particle will be practically zero.

Likewise, for a very long pore ($H \gg Q$ in Fig. 2) and a comparatively short particle ($L \ll H$) with both ends far inside the pore, an almost translation invariant net force on the particle is expected (the pore ends hardly matter). Furthermore, for symmetry reasons the forces acting onto either end of the particle will almost cancel each other, i.e., a close to zero net force is expected.

The main focus of the present section is on the following mixture of the above two cases: We consider a very long pore ($H \gg Q$ in Fig. 2) in combination with a sufficiently long particle ($L \gg Q$), so that one of its ends is far inside the pore and the other end far outside the pore. Again, one thus expects an almost translation invariant net force on the particle, but now there is no symmetry argument that this constant force should be almost zero. Rather one expects that the force will actually be (almost) maximal (in modulus). In the following, our main goal is to analytically approximate this maximum force, henceforth denoted as F^m.

Closer inspection of the surface integrals in Eqs. (16) and (23) shows that, as expected from our above considerations, the main contributions to F^m are generated in the vicinity of the particle's end far inside the pore. Since no analytical (exact or approximate) solutions of the Poisson-Boltzmann

equation (22) seem to exist for such a case, we cannot evaluate the surface integrals (16), (23) directly. We therefore adopt the following, alternative approach: We assume that the particle is moved an infinitesimal distance Δz into the pore (along the cylinder axis). Accordingly, the free energy of the system will change by an amount ΔG. The force F^m required to hold the particle fixed at the initial position is thus given by

$$F^m = -\Delta G/\Delta z. \tag{27}$$

In the framework of the Poisson-Boltzmann equation (22) the free energy of the system can be expressed in several equivalent forms [43,47]. The most convenient form for our purpose is

$$G = \int_V d\mathbf{x} \left[\frac{\rho_m(\mathbf{x}) - \rho(\mathbf{x})}{2} \psi(\mathbf{x}) - p(\mathbf{x}) \right], \tag{28}$$

where the integration domain V is the entire fluid chamber. Since $H, L \gg Q$, we can approximate the free energy difference as

$$\Delta G \approx (g_2 - g_1)\Delta z, \tag{29}$$

and hence F^m from (27) as

$$F^m \approx g_1 - g_2, \tag{30}$$

where g_1 is the free energy per unit length for an infinitely long, empty pore, and g_2 is the corresponding free energy per unit length for an infinitely long particle in an infinitely long pore. For both situations the potentials $\psi_{1,2}$ and the charge densities $\rho_{1,2}$ become independent of z. We may thus adopt cylinder coordinates with $r := (|\mathbf{x}|^2 - z^2)^{1/2}$ and rewrite the Poisson-Boltzmann equation (22) as

$$\frac{1}{r}\frac{d}{dr}\left(r \frac{d}{dr} \psi_{1,2}(r) \right) = -\frac{2Ze_0 N_A c_0}{\epsilon_0 \epsilon_w} \sinh\left(\frac{Ze_0 \psi_{1,2}(r)}{k_B T} \right), \tag{31}$$

complemented by the conditions $\psi_{1,2}(r) = 0$ for $r > Q$ [overall charge neutrality of pore surface and counterions, cf. Eq. (1) and convention $\psi_{1,2}(r \to \infty) = 0$], $\psi'_{1,2}(r = Q) = \sigma/\epsilon_0\epsilon_w$ [cf. Eq. (9)], $\psi'_1(r = 0) = 0$ (regularity at the pore center), $\psi'_2(r = R) = 0$ [cf. Eq. (10)], and $\psi'_2(r) = 0$ for $r < R$ [cf. Eq. (1)].

While Eq. (31) still cannot be solved analytically in full generality, we will focus on approximations for two limiting cases in the following two subsections.

Once the latter problem is solved, we can exploit that $\rho(\mathbf{x}) = 0$ outside the electrolyte solution and that $\rho_m(r) = \sigma\delta(r - Q)$ to calculate the free energy per unit length according to Eq. (28) as

$$g_i = \pi\sigma Q \psi_i(Q) - \int_{l_i}^{Q} dr\, 2\pi r \left[\frac{\rho_i(r)\psi_i(r)}{2} + p_i(r) \right] \tag{32}$$

with $l_1 = 0$ and $l_2 = R$. Finally, F^m follows according to (30).

A. High concentration or low surface charge

We first focus on the so-called Debye-Hückel limit $Ze_0|\psi_i(r)|/k_B T \lesssim 1$ throughout the nanopore, which is tantamount to low surface charge densities σ and/or high bulk concentrations c_0. The corresponding approximation for the the maximum force F^m from (30) is henceforth denoted as F^m_l. Referring to the Appendix A for the detailed calculation, the final result is

$$F^m_l = \frac{\pi\sigma^2 Q}{\epsilon_0\epsilon_w\kappa} \left(\frac{I_0(\kappa r)}{I_1(\kappa Q)} - \frac{I_0(\kappa r)K_1(\kappa R) + K_0(\kappa r)I_1(\kappa R)}{K_1(\kappa R)I_1(\kappa Q) - I_1(\kappa R)K_1(\kappa Q)} \right) \tag{33}$$

where $\kappa := \lambda_D^{-1}$ is the inverse Debye length from (11) and I_k (K_k) is the modified Bessel function of the first (second) kind and order k.

Likewise, for the electric field and the pressure in the empty pore (index 1) the following approximations are derived in Appendix A:

$$\psi_1(r) = \frac{\sigma}{\epsilon_0\epsilon_w\kappa} \frac{I_0(\kappa r)}{I_1(\kappa Q)} \tag{34}$$

$$p_1(r) = \frac{N_A c_0}{k_B T} \left(\frac{Ze_0\sigma}{\epsilon_0\epsilon_w\kappa} \frac{I_0(\kappa r)}{I_1(\kappa Q)} \right)^2. \tag{35}$$

B. Low concentration or high surface charge

Next we turn to the case $Ze_0|\psi_i(r)|/k_B T \gtrsim 1$, i.e., high surface charge densities σ and/or low concentrations c_0. Hence, we follow Philip and Wooding [44] and exploit the approximation

$$\sinh\left(\frac{Ze_0\psi_i(r)}{k_B T} \right) \approx \frac{\mathrm{sign}(\psi_i(r))}{2} \exp\left(\frac{Ze_0|\psi_i(r)|}{k_B T} \right). \tag{36}$$

Making use of $\mathrm{sign}[\psi_i(r)] = \mathrm{sign}(\sigma)$ and hence $|\psi_i(r)| = \mathrm{sign}(\sigma)\psi_i(r)$, the first solution ($\psi_1$) of Eq. (31) with the boundary conditions discussed below (31) is

$$\psi_1(r) = -\mathrm{sign}(\sigma) U_0 \left(\ln\left[\frac{c_0 Ze_0 N_A a_1}{a_2} \right] + 2\ln\left[1 - \frac{Ze_0|\sigma|r^2}{a_1} \right] \right), \tag{37}$$

where we have defined

$$U_0 := \frac{k_B T}{Ze_0}, \tag{38}$$

$$a_1 := Q(4\epsilon_0\epsilon_w k_B T + Ze_0|\sigma|Q), \tag{39}$$

$$a_2 := 8\epsilon_0\epsilon_w k_B T|\sigma|. \tag{40}$$

The somewhat more lengthy expressions for $\psi_2(r)$ are provided in Appendix B.

Given $\psi_i(r)$, the pressure and the charge density follow from (20), (21). With (36) and an analogous approximation for $\cosh(\cdot)$, they take the form

$$\rho_i(r) = -\mathrm{sign}(\sigma) Ze_0 N_A c_0 \exp\left\{ \frac{\mathrm{sign}(\sigma)\psi_i(r)}{U_0} \right\}, \tag{41}$$

$$p_i(r) = k_B T N_A c_0 \exp\left\{ \frac{\mathrm{sign}(\sigma)\psi_i(r)}{U_0} \right\}. \tag{42}$$

Finally, by exploiting the above results to evaluate the integral (32) we arrive at our final approximation for the maximum force F^m from (30), henceforth denoted as F^m_g. An interesting property of this approximation F^m_g is demonstrated

in Appendix C, namely that it is independent of the bulk concentration c_0.

V. NUMERICAL RESULTS

A. Empty pore

As a first example we consider the case of an empty pore (Fig. 2 without particle). Assuming a typical membrane surface charge density of $\sigma = -50\ \mathrm{mC/m^2}$ and a relatively low bulk concentration of $c_0 = 1$ mM (cf. Sec. II), we have numerically solved the Poisson-Boltzmann equation (22) as detailed in Sec. III E.

Figure 3 illustrates the results for the electric potential $\psi(\mathbf{x})$ and for the corresponding pressure $p(\mathbf{x})$ from (20). Most remarkably, the pressure within the pore increases quite notably beyond the bulk value $p_0 = 0$ Pa from Eq. (13). In fact, the counterion pressure near the membrane surface typically may become as large as 20 bar according to Figs. 3(d), 3(f), 3(h).

For a cross section through the $z = 0$ plane (i.e., through the pore center), Figs. 3(c) and 3(d) provide a more detailed picture of the numerically obtained fields for $c_0 = 1$ mM together with the analytical approximations (37) and (42) for low concentrations.

We found a comparably good agreement even for a tenfold increased bulk concentration, i.e., for $c_0 = 10$ mM (not shown). Significant deviations arise upon another tenfold increased concentration, i.e., for $c_0 = 100$ mM, see red lines in Figs. 3(e) and 3(f). Finally, for $c_0 = 1000$ mM, the analytical approximation for low concentrations is far off the numerics from Figs. 3(g) and 3(h).

Likewise, the approximations (34) and (35) for high bulk concentrations reproduce the numerical solution almost perfectly for $c_0 = 1000$ mM [blue lines in Figs. 3(g) and 3(h)], develop notable deviations for $c_0 = 100$ mM [Figs. 3(e) and 3(f)], and completely fail for $c_0 = 10$ mM and $c_0 = 1$ mM.

B. Force on the particle

What happens when an uncharged particle approaches and enters the previously considered empty pore? On the one hand, the electric potential in Fig. 3(a) induces a polarization of the particle, which, due to the higher polarizability of the ambient liquid, results in a net repulsion, see Fig. 1(a). On the other hand, the counterion pressure in Fig. 3(b) generates yet another repulsive force contribution, see Fig. 1(b). Strictly speaking, there will also be back reactions of the approaching particle on the unperturbed electric and pressure fields of the empty pore from Fig. 3, but these are next-to-leading-order effects, which may be neglected for our present purpose of a basic understanding of the main mechanisms.

Similarly as at the beginning of Sec. IV, both these forces are expected to develop certain plateau regions for sufficiently long pores or particles. Concerning a more quantitative understanding, especially with respect to the relative importance of the two forces, integrating the different contributions over the entire particle volume or surface [essentially as in Eqs. (16) and (23)] is unavoidable and goes beyond the realm of simple intuitive arguments.

Figure 4 exemplifies the numerically obtained forces for four different particle lengths L and two different bulk concentrations c_0. Qualitatively, these results are very similar

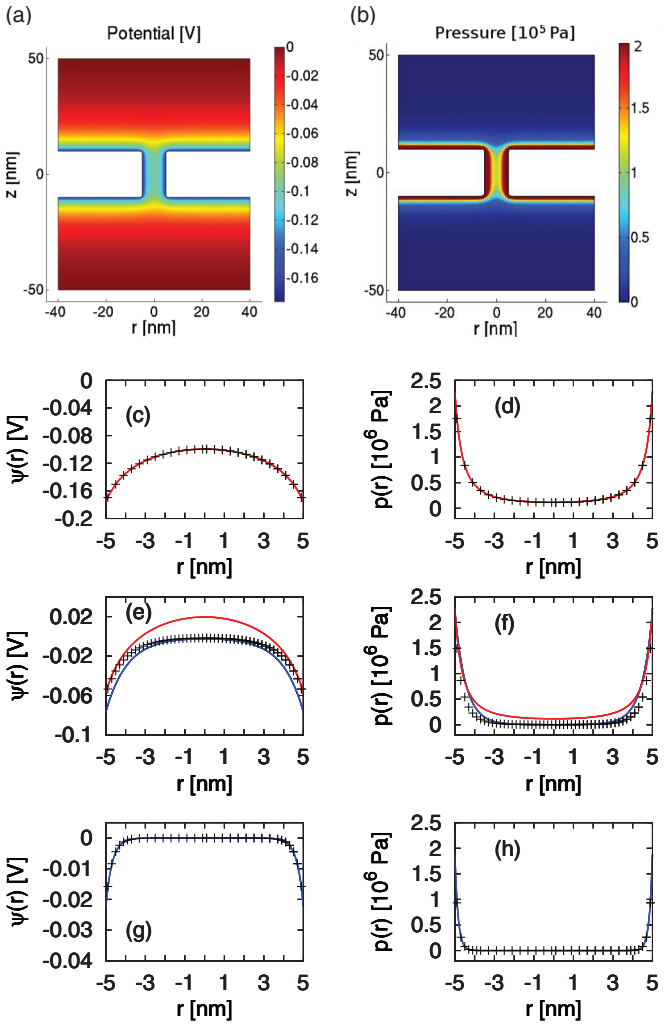

FIG. 3. (Color online) (a) Electric potential $\psi(r,z)$ by numerically solving the Poisson-Boltzmann equation (22) for an empty pore (cf. Fig. 2) with radius $Q = 5$ nm, membrane thickness $H = 20$ nm, surface charge density $\sigma = -50\,\mathrm{mC/m^2}$, bulk concentration $c_0 = 1$ mM, and dielectric constants $\epsilon_w = 80$, $\epsilon_m = \epsilon_p = 5$ [cf. Eqs. (7)–(10)]. (b) Corresponding pressure from (20). All pressures beyond 2×10^5 Pa are displayed in deep red [see also (d)]. (c) and (d): Radial dependence of the same fields for $z = 0$ (i.e., in the middle of the pore), obtained numerically (symbols) and by means of the analytical approximations (34) and (35) for low concentrations (red lines). The units in (d) are now 10^6 Pa. (e) and (f): Same, but for $c_0 = 100$ mM. In addition, the analytical approximations (37) and (42) for high concentrations are shown as blue (lower) lines. (g) and (h): Same, but for $c_0 = 1000$ mM.

for both bulk concentrations, but the absolute values of the forces are approximately a decade larger for $c_0 = 10$ mM than for $c_0 = 100$ mM. Further main observations are:

(i) Although the particle is neutral, the dielectric force $F_e(z)$ does not vanish [Figs. 4(c) and 4(d)].

(ii) The z dependence of this dielectric force is quite complicated, in particular if $L \approx H$, see Fig. 2 and the green and blue lines in Figs. 4(c) and 4(d).

(iii) The hydrodynamic force $F_h(z)$ generated by the counterion pressure [see below (23)] is much larger than the dielectric force $F_e(z)$.

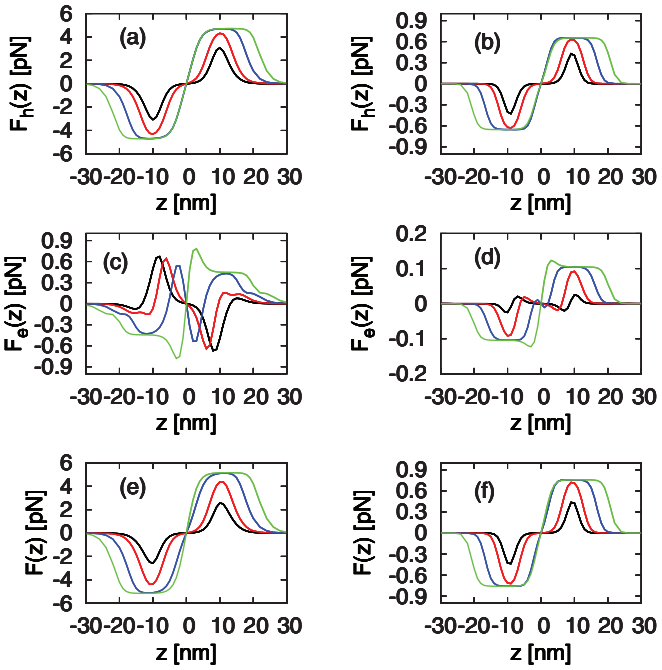

FIG. 4. (Color online) Numerically obtained results (in units of pN) versus z (in units of nm) for the z components $F_e(z)$, $F_h(z)$, and $F(z)$ of the dielectric force (16), the counterion pressure force (23), and the total force (15), respectively, when the particle center in Fig. 2 finds itself at an arbitrary but fixed position z along the pore axis. The different curves represent results for particles with fixed radius $R = 3$ nm and various lengths, namely $L = 6$ nm (black), $L = 10$ nm (red), $L = 18$ nm (blue), and $L = 26$ nm (green). [Overall, the forces increase (in modulus) with particle length.] The pore radius was $Q = 5$ nm, the membrane thickness $H = 20$ nm, the surface charge density $\sigma = -50$ mC/m^2, and the concentration $c_0 = 10$ mM in (a), (c), (e), and $c_0 = 100$ mM in (b), (d), (f). The dielectric constants in Eq. (7) were $\epsilon_w = 80$ and $\epsilon_m = \epsilon_p = 5$.

(iv) The various above predicted force plateaus are indeed observed. In particular, the total force $F(z)$ develops for sufficiently large particle lengths L two symmetric, asymptotically L-independent plateaus $\pm F^m$ [Figs. 4(e) and 4(f)], for which we derived the analytical approximations F_l^m in Eq. (33) and F_g^m in Sec. IV B.

Figure 5(a) shows the maximum force F^m as a function of the bulk concentration c_0 for a fixed surface charge density $\sigma = -50$mC/m^2. More precisely, the numerical results were obtained by solving the Poisson-Boltzmann equation (22) for an $L = 60$ nm long particle at $z = 30$ nm, i.e., with its lower end at the center of the nanopore. The numerical solution compares very well with the two complementary asymptotic approximations F_l^m from (33) and F_g^m from Sec. IV B. In particular, the maximum force F^m becomes (almost) constant for low c_0, as predicted at the end of Sec. IV B.

Analogously, in Fig. 5(b) the surface charge density was varied while keeping the concentration c_0 fixed at 10 mM. In particular, F^m indeed scales with σ^2 for sufficiently low surface charge densities σ, as predicted by the analytical approximation (33) (blue line).

Summarizing Fig. 5, we can say that the maximum force is well approximated by F_l^m for low charge densities σ and/or high concentrations c_0, and by F_g^m for high charge densities and/or low concentrations. Figures 5(a) and 5(b) also suggest that for arbitrary σ and c_0, at least one of the two approximations F_l^m or F_g^m always works reasonably well. We furthermore observe that $F_l^m \ll F_g^m$ in case that F_l^m is a good approximation and that $F_g^m \ll F_l^m$ in the regime of validity of the approximation F_g^m. This suggests the following empirical interpolation formula for the maximum force

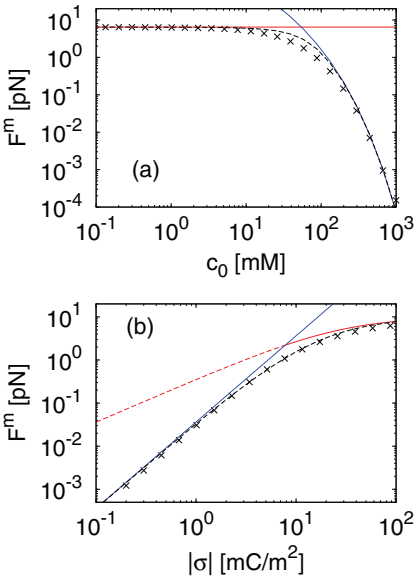

FIG. 5. (Color online) The maximum (or plateau) force F^m (in units of pN) for the same system as in Figs. 4(a), 4(c), and 4(e), but now for a particle length of $L = 60$ nm and a variable bulk concentration c_0 (in units of mM) in (a) and a variable (negative) surface charge density $\sigma = -|\sigma|$ (in units of mC/m^2) in (b). Symbols: Numerical solutions. Red lines [horizontal in (a), partially dashed in (b)]: Approximation F_g^m for low concentration or high surface charge from Sec. IV B. Blue lines: Approximation F_h^m from (33) for high concentration or low surface charge. Dashed: Empirical interpolation (43) between these to approximations. In (b) the red solid line corresponds to case "+" in Eq. (B1) and its dashed continuation to case "−".

$$F^m_{\rm emp} = \left(\frac{1}{F_l^m} + \frac{1}{F_g^m}\right)^{-1}. \tag{43}$$

The dashed lines in Fig. 5 show that this approximate crossover formula indeed works remarkably well for arbitrary concentrations and charge densities.

C. Potential barriers against entering the pore

Figure 6 exemplifies the potential $U(z)$ and, in particular, the potential barriers ΔU governing the pore entrance and translocation by a nanoparticle. While barriers up to a few k_BT may still be surmounted by thermal activation within reasonable time scales, larger barriers practically rule out a translocation through the pore in view of the typical Boltzmann-Arrhenius factors $\exp(-\Delta U/k_BT)$ by which thermally activated rate processes are ruled [45]. In conclusion, the translocation of neutral particles through nanopores can be greatly suppressed if the nanopore walls carry surface charges.

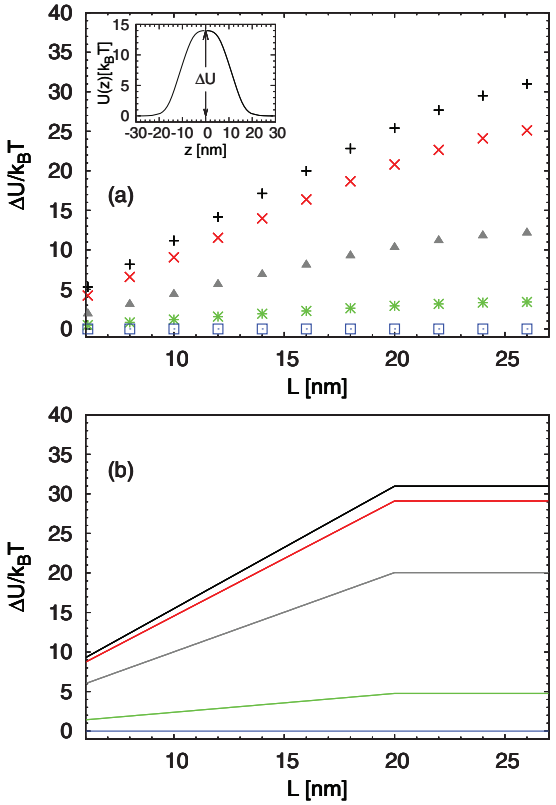

FIG. 6. (Color online) (a) *Inset*: The potential energy $U(z)$ in units of the thermal energy k_BT versus z (in units of nm), obtained numerically from Eqs. (15), (16), (23), and (24), for a particle length $L = 14$ nm and all other parameters as in Figs. 4(a), 4(c), and 4(e). The potential barrier ΔU is indicated by the double arrow. Main figure: Potential barrier ΔU (in units of k_BT) versus particle length L (in units of nm) for five different bulk concentrations c_0, namely (top-down) 1 mM (black), 10 mM (red), 40 mM (gray), 100 mM (green), and 1000 mM (blue). (b) The corresponding analytical estimates from (43) and (44).

According to Figs. 4 and 5 and their discussion in the main text, the force $F(z)$ develops two plateaus of height $\pm F^m$, whose widths can be very roughly approximated as $\min\{L, H\}$. In combination with (24) and (43) we thus arrive at the following approximation for the potential barrier,

$$\Delta U_{\text{emp}} = F^m_{\text{emp}} \min\{L, H\}. \tag{44}$$

As Fig. 6 demonstrates, this simple approximation reproduced the numerically obtained barriers quite well. The deviations are mainly rooted in the fact that we cannot approximate very well the edges of the force plateaux in Figs. 4(e) and 4(f).

D. Generalizations

So far, we have restricted ourselves to particles with radii $R = 3$ nm. We have seen that, beside other factors, the potential barrier for crossing the pore strongly depends on the ion concentrations. Above $c_0 \approx 100$ mM the barrier nearly vanishes. For these salt concentrations, the distance of the particle from the wall, $Q - R$, is larger than a few times the Debye length λ_D from (11) so that the surface charge is almost entirely screened by the counterions. On the other hand, if $Q - R$ is comparable to or smaller than the Debye length, the counterion pressure within the nanopore will significantly influence the translocation dynamics. For particle radii other than $R = 3$ nm, all effects will thus be qualitatively the same as for particles with $R = 3$ nm, if the pore radius and/or the concentration are adapted accordingly.

Next we briefly discuss how the results from Sec. V B depend on the surface charge density σ. As tacitly anticipated in Fig. 5(b), all forces are obviously independent of the sign of those charges, i.e., they must be even functions of σ. Moreover, they must vanish in the absence of any surface charges. Hence, the leading order behavior for small σ will be proportional to σ^2. This asymptotics as well the behavior beyond the small σ regime is illustrated by Fig. 5(b). Moreover, we found numerically, e.g., for $\sigma = -20\,\text{mC/m}^2$ almost the same shapes of the force curves as for $\sigma = -50\,\text{mC/m}^2$ in Fig. 4, just their overall amplitudes were rescaled by the same factor of ≈ 0.5 as the corresponding maximum force F^m in Fig. 5(b). A similar behavior is expected for a large range of other σ values.

While the surface charge density of sulfate coated surfaces is, e.g., quite independent of the solution conditions [17,21], the surface charge density of silica (SiO_2) membranes has been reported to increase with increasing concentration c_0 and has typical values between $-10\,\text{mC/m}^2$ and $-100\,\text{mC/m}^2$ for c_0 between 1 mM and 1000 mM [17,20–22,46]. In such a case, a more realistic modeling should take into account a reduction of the surface charge density within the pore, compared to the membrane charge density far from the pore [17]. We have conducted preliminary numerical investigations along these lines, indicating that the results change only quite insignificantly.

VI. CONCLUSIONS

We have explored the forces, experienced by an electrically neutral but in general polarizable nanorod in an electrolyte solution, which are generated by a constant surface charge density on a membrane with a cylindrical nanopore. Unless the Debye screening length (11), quantifying the characteristic extension of the electric double layer, is much smaller than the minimal distance between particle and pore walls, those forces are quite notable and give rise to significant potential barriers against the particle's entrance into the pore. The dominating contribution is due to the mutual repulsion of the counterions, which screen the surface charges, resulting in an repulsive pressure force on those parts of the particle which are entering the counterion cloud. A second contribution is due to the combined net effect of all the induced dipoles in the particle and the ambient fluid. Under typical experimental conditions those dielectric forces are, however, much weaker than the counterion pressure forces. This is in striking contrast to the extensively studied opposite case of a charged particle, entering a neutral pore [2–6].

What happens if both the pore and the particle are charged? While a systematic exploration of this issue goes beyond the scope of our present paper, we briefly may point out the main features of our numerical findings in the special case that the pore and the particle both carried the same surface charge $\sigma = -50\,\text{mC/m}^2$ [all other parameters as in Figs. 4(a), 4(c), and 4(e)]: The forces $F_h(z)$ exhibited almost the same shapes

as those in Fig. 4(a), while their amplitudes increased by about a factor of five. The forces $F_e(z)$ did not resemble those from Fig. 4(b) at all, rather they now were almost (but not exactly) proportional to $F_h(z)$ with proportionality constants close to unity. As a consequence, also the total forces $F(z)$ were similar to those from Fig. 4(e), except that the amplitudes were larger by about a factor of ten. In particular, these findings cannot be understood by simply superimposing the cases of an uncharged particle and of an uncharged pore. We also note that while F_h can still be associated with the counterion pressure effects [cf. Fig. 1(b) and Eq. (23)], F_e now comprises not only the dielectric forces, but also the only partially screened electrostatic repulsion between the equally charged particle and pore walls [cf. Fig. 1(a) and Sec. III C].

Regarding potential applications, a particularly interesting direction may be ultrafiltration [41], especially the design of sieves for uncharged (and possibly even nonpolarizable) nanoparticles, whose particle sorting characteristics can be adjusted by means of the ion concentration, see Fig. 6.

ACKNOWLEDGMENT

This work was supported by Deutsche Forschungsgemeinschaft under SFB 613 and RE1344/8-1 and by the Paderborn Center for Parallel Computing.

APPENDIX A

In this Appendix we provide the derivation of the approximations (33)–(35).

Exploiting $\sinh(x) \approx x$ for $|x| \lesssim 1$ yields the Poisson-Boltzmann equation (31) in the Debye-Hückel limit

$$\frac{1}{r}\frac{d}{dr}\left(r\frac{d}{dr}\psi_i(r)\right) = \kappa^2\psi_i(r), \tag{A1}$$

where $\kappa := \lambda_D^{-1}$ is the inverse Debye length, see (11).

By exploiting the above approximation $\sinh(x) \approx x$ for $|x| \lesssim 1$ once again in Eq. (21) and the analogous approximation $\cosh(x) \approx 1 + x^2/2$ for $|x| \lesssim 1$ in Eq. (20), we obtain

$$\rho_i(r) = -2Ze_0N_Ac_0\frac{Ze_0\psi_i(r)}{k_BT} \tag{A2}$$

$$p_i(r) = k_BTN_Ac_0\left(\frac{Ze_0\psi_i(r)}{k_BT}\right)^2. \tag{A3}$$

As a consequence, the integrand in Eq. (32) vanishes and the free energy per unit length simplifies to [47]

$$g_i = \pi\sigma Q\psi_i(Q). \tag{A4}$$

The solutions of Eq. (A1) with the boundary conditions discussed below Eq. (31) are well known (see, e.g., Refs. [48,49]) and are given by (34) and

$$\psi_2(r) = \frac{\sigma}{\epsilon_0\epsilon_w\kappa}\frac{I_0(\kappa r)K_1(\kappa R) + K_0(\kappa r)I_1(\kappa R)}{K_1(\kappa R)I_1(\kappa Q) - I_1(\kappa R)K_1(\kappa Q)}, \tag{A5}$$

where I_k (K_k) is the modified Bessel function of the first (second) kind and order k.

Introducing (34) and (A5) into (A4) and (30) yields (33). Introducing (34) into (A3) yields (35).

APPENDIX B

In this Appendix we provide the analytical solution $\psi_2(r)$ of the Poisson-Boltzmann equation (31) within the approximation (36), originally derived in Refs. [44,50], and assuming different functional forms, depending on the model parameters:

$$\psi_2(r) = \begin{cases} \psi_+(r) & \text{if } \ln\frac{Q}{R} < 1 \text{ and } |\sigma| > \frac{2U_0\epsilon_0\epsilon_w\ln\frac{Q}{R}}{Q(1-\ln\frac{Q}{R})} \\ \psi_-(r) & \text{else} \end{cases}. \tag{B1}$$

The function ψ_+ is given by

$$\psi_+(r) := \operatorname{sign}(\sigma)U_0\ln\left(\frac{-a_3}{\kappa^2r^2\cos^2\left(a_4 + \frac{1}{2}\sqrt{-a_3}\ln\frac{r}{R}\right)}\right), \tag{B2}$$

where κ is the inverse Debye length (11) and where U_0 is given by (38).

The potential ψ_+ has to satisfy the boundary conditions discussed below Eq. (31), which fix the parameters a_3 and a_4. A straightforward calculation shows that a_3 is thus given by

$$a_3 := -4/\tan^2(a_4) \tag{B3}$$

and that a_4 is implicitely given as the solution of

$$\cot(a_4)\tan\left(a_4 + \cot(a_4)\ln\frac{Q}{R}\right) = 1 + \frac{Q|\sigma|}{2U_0\epsilon_0\epsilon_w} \tag{B4}$$

in the interval $(a_{\min},\pi/2)$ where $a_{\min} > 0$ is implicitly defined via

$$(\pi/2 - a_{\min})\tan(a_{\min}) = \ln Q/R. \tag{B5}$$

Analogously, ψ_- is given by

$$\psi_-(r) := \operatorname{sign}(\sigma)U_0\ln\left(\frac{4a_5a_6(\kappa r)^{\sqrt{a_6}}}{(\kappa r)^2[1 - a_5(\kappa r)^{\sqrt{a_6}}]^2}\right) \tag{B6}$$

with

$$a_5 := \frac{2 - \sqrt{a_6}}{(2 + \sqrt{a_6})(\kappa R)^{\sqrt{a_6}}} \tag{B7}$$

and $a_6 \in (0,4)$ being implicitly defined via

$$\frac{(a_6 - 4)\left[1 - \left(\frac{Q}{R}\right)^{\sqrt{a_6}}\right]}{(2 + \sqrt{a_6}) - (2 - \sqrt{a_6})\left(\frac{Q}{R}\right)^{\sqrt{a_6}}} = \frac{|\sigma|Q}{U_0\epsilon_0\epsilon_w}. \tag{B8}$$

APPENDIX C

In this Appendix we show that the approximation F_g^m from Sec. IV B is independent of the bulk concentration c_0.

Introducing (37) into (41) and (42) it follows that both $p_1(r)$ and $\rho_1(r)$ are independent of c_0. The free energy per unit length g_1 thus follows with Eq. (32) and (37) as

$$g_1 = -\operatorname{sign}(\sigma)\pi U_0\ln(c_0)\left[Q\sigma - \int_0^Q dr\, r\rho(r)\right] + \cdots, \tag{C1}$$

where the dots refer to terms which are independent of c_0. Multiplying the integral in Eq. (C1) by 2π yields the charge per unit length due to the mobile ions. Employing the Gauss theorem [1] and the boundary conditions discussed below Eq. (31) shows that the integral equals $-Q\sigma$ and hence

$$g_1 = -2\text{sign}(\sigma)\pi U_0 \ln(c_0) Q\sigma + \cdots. \tag{C2}$$

Analogously, it can be shown that also g_2 from (32) is of the form

$$g_2 = -2\text{sign}(\sigma)\pi U_0 \ln(c_0) Q\sigma + \cdots, \tag{C3}$$

where the dots in Eqs. (C2) and (C3) indicate in general two different terms, both of which are however independent of c_0. We thus can conclude that the maximum force F_g^m from (30) is independent of c_0 as well.

[1] J. D. Jackson, *Classical Electrodynamics* (Wiley, New York, 1999).

[2] A. Parsegian, Nature (London) **221**, 844 (1969); Ann. NY Acad. Sci. **264**, 161 (1975); D. G. Levitt, Biophys. J. **22**, 209 (1978); P. C. Jordan, *ibid*. **39**, 157 (1982); S. Teber, J. Stat. Mech.: Theory Exp. (2005) P07001.

[3] P. C. Jordan, R. J. Bacquet, J. A. McCammon, and P. Tran, Biophys. J. **55**, 1041 (1989); A. G. Cherstvy, J. Phys. Chem. B **110**, 14503 (2006).

[4] J. Zhang and B. I. Shklovskii, Phys. Rev. E **75**, 021906 (2007).

[5] D. J. Bonthuis, J. Zhang, B. Hornblower, J. Mathé, B. I. Shklovskii, and A. Meller, Phys. Rev. Lett. **97**, 128104 (2006).

[6] S. Kesselheim, M. Sega, and C. Holm, Comput. Phys. Commun. **182**, 33 (2011); Soft Matter **8**, 9480 (2012).

[7] J. E. Sader and D. Y. C. Chan, Langmuir **16**, 324 (2000).

[8] A. Meller, J. Phys.: Condens. Matter **15**, R581 (2003).

[9] J. J. Kasianowicz, E. Brandin, D. Branton, and D. W. Deamer, Proc. Nat. Acad. Sci. USA **93**, 13770 (1996).

[10] A. Meller, L. Nivon, and D. Branton, Phys. Rev. Lett. **86**, 3435 (2001).

[11] T. Z. Butler, J. H. Gundlach, and M. A. Troll, Biophys. J. **93**, 3229 (2007).

[12] C. Dekker, Nature Nanotechnol. **2**, 209 (2007); D. Branton *et al*., *ibid*. **26**, 1146 (2008); M. Zwolak and M. Di Ventra, Rev. Mod. Phys. **80**, 141 (2008); S. Howorka and Z. Siwy, Chem. Soc. Rev. **38**, 2360 (2009); A. Aksimentiev, Nanoscale **2**, 468 (2010); B. M. Venkatesan and R. Bashir, Nat. Nanotechnol. **6**, 615 (2011).

[13] A. J. Storm, C. Storm, J. Chen, H. Zandbergen, J. Joanny, and C. Dekker, Nano Lett. **5**, 1193 (2005).

[14] M. Wanunu, J. Sutin, B. McNally, A. Chow, and A. Meller, Biophys. J. **95**, 4716 (2008).

[15] A. Spiering, S. Getfert, A. Sischka, P. Reimann, and D. Anselmetti, Nano Lett. **11**, 2978 (2011).

[16] R. F. Probstein, *Physicochemical Hydrodynamics* (Wiley-Interscience, Hoboken, NJ, 2003).

[17] S. H. Behrens and D. G. Grier, J. Chem Phys. **115**, 6716 (2001).

[18] D. Stein, M. Kruithof, and C. Dekker, Phys. Rev. Lett. **93**, 035901 (2004).

[19] Y. He, M. Tsutsui, C. Fan, M. Taniguchi, and T. Kawai, ACS Nano **5**, 5509 (2011).

[20] B. J. Kirby and E. F. Hasselbrink, Electrophoresis **25**, 187 (2004).

[21] M. B. Andersen, J. Frey, S. Pennathur, and H. Bruus, J. Colloid Interface Sci. **353**, 301 (2011).

[22] D. P. Hoogerheide, S. Garaj, and J. A. Golovchenko, Phys. Rev. Lett. **102**, 256804 (2009).

[23] Y. Ai, J. Liu, B. Zhang, and S. Qian, Anal. Chem. **82**, 8217 (2010).

[24] M. Zhang, L. Yeh, S. Qian, J. Hsu, and S. W. Joo, J. Phys. Chem. C **116**, 4793 (2012).

[25] Y. Ai and S. Qian, Phys. Chem. Chem. Phys. **13**, 4060 (2011).

[26] L. Chen and A. T. Conslik, Biomed. Microdevices **12**, 235 (2010).

[27] B. Luan and A. Aksimentiev, J. Phys.: Condens. Matter **22**, 454123 (2010).

[28] B. Luan and A. Aksimentiev, Phys. Rev. E **78**, 021912 (2008).

[29] D. K. Lubensky and D. R. Nelson, Biophys. J. **77**, 1824 (1999); P. Reimann, Phys. Rep. **361**, 57 (2002); M. Muthukumar and C. Y. Kong, PNAS **103**, 5273 (2006).

[30] R. S. Eisenberg, J. Membr. Biol. **150**, 1 (1996).

[31] B. Corry, S. Kuyucak, and S. Chung, Biophys. J. **78**, 2364 (2000).

[32] J. H. Masliyah and S. Bhattacharjee, *Electrokinetic and Colloidal Transport Phenomena* (Wiley-Interscience, Hoboken, NJ, 2006).

[33] J. Zhang, A. Kamenev, and B. I. Shklovskii, Phys. Rev. Lett. **95**, 148101 (2005).

[34] L. Chen and A. T. Conslik, Biomed. Microdevices **10**, 289 (2008).

[35] S. van Dorp, U. F. Keyser, N. H. Dekker, C. Dekker, and S. G. Lemay, Nature Phys. **5**, 347 (2009).

[36] S. Das, P. Dubsky, A. van den Berg, and J. C. T. Eijkel, Phys. Rev. Lett. **108**, 138101 (2012).

[37] R. L. Panton, *Incompressible Flow*, 3rd ed. (John Wiley & Sons, Inc., Hoboken, NJ, 2005).

[38] COMSOL, *Comsol Multiphysics Reference Guide* (2012), Chap. 7.

[39] L. Chen and A. T. Conlisk, Biomed. Microdevices **13**, 403 (2011).

[40] P. K. Das, S. Bhattacharjee, and W. Moussa, Langmuir **19**, 4162 (2003).

[41] W. R. Bowen and A. O. Sharif, Proc. R. Soc. London A **452**, 2121 (1996)

[42] S. Getfert, T. Töws, and P. Reimann, Phys. Rev. E **87**, 062710 (2013).

[43] E. S. Reiner and C. J. Radke, AIChE J. **37**, 805 (1991).

[44] J. R. Philip and R. A. Wooding, J. Chem. Phys. **52**, 953 (1970).

[45] P. Hänggi, P. Talkner, and M. Borkovec, Rev. Mod. Phys. **62**, 251 (1990).

[46] F. H. J. van der Heyden, D. Stein, and C. Dekker, Phys. Rev. Lett. **95**, 116104 (2005).

[47] K. A. Sharp and B. Honig, J. Phys. Chem. **94**, 7684 (1990).

[48] C. L. Rice and R. Whitehead, J. Phys. Chem. **69**, 4017 (1965).

[49] S. Ghosal, Phys. Rev. E **76**, 061916 (2007).

[50] S. Levine, J. R. Marriott, G. Neale, and N. Epstein, J. Colloid. Interface Sci. **52**, 136 (1975).